Journal of *Marine Science and Engineering*

MDPI

Article

Multiple Autonomous Underwater Vehicle Formation Obstacle Avoidance Control Using Event-Triggered Model Predictive Control

Linling Wang [1], Xiaoyan Xu [1,*], Bing Han [2,3] and Huapeng Zhang [4]

[1] Shanghai Engineering Research Center of Intelligent Maritime Search & Rescue and Underwater Vehicles, Shanghai Maritime University, Shanghai 201306, China; 202140210013@stu.shmtu.edu.cn
[2] College of Physics and Electronic Information Engineering, Minjiang University, Fuzhou 350108, China; han.bing@coscoshipping.com
[3] Shanghai Ship and Shipping Research Institute Co., Ltd., Shanghai 200131, China
[4] Department of Automation, Shanghai Jiao Tong University, Shanghai 200240, China; 909934239@stju.edu.cn
* Correspondence: xuxy@shmtu.edu.cn

Abstract: In this paper, multiple autonomous underwater vehicle (multi-AUV) formation control with obstacle avoidance ability in 3D complex underwater environments based on an event-triggered model predictive control (EMPC) is proposed. Firstly, multi-AUV motion model systems are developed. The navigation reference trajectory of the follower AUVs can be obtained using a multi-AUV relative motion model. Secondly, in order to overcome the speed jump and obstacle avoidance problem in multi-AUV systems, compatibility constraints are presented in MPC that limit the uncertainty deviation of each AUV. The event-triggered mechanism (ET) is designed to decrease the computational load, which is based on the error between the optimal predicted and current state of the AUV. Finally, the effectiveness and superiority of the proposed algorithm are confirmed via simulation and compared with those of other algorithms.

Keywords: event triggered; leader-follower; multi-AUV; MPC; obstacle avoidance

Citation: Wang, L.; Xu, X.; Han, B.; Zhang, H. Multiple Autonomous Underwater Vehicle Formation Obstacle Avoidance Control Using Event-Triggered Model Predictive Control. *J. Mar. Sci. Eng.* **2023**, *11*, 2016. https://doi.org/10.3390/jmse11102016

Academic Editor: Leszek Chybowski

Received: 28 July 2023
Revised: 4 October 2023
Accepted: 6 October 2023
Published: 19 October 2023

1. Introduction

In the complex and changeable marine environment, how to use the autonomous underwater vehicle (AUV) to carry out maritime search and rescue, environmental investigation, surveillance and reconnaissance, anti-submarine, environmental monitoring, and other search behaviors is a subject worthy of being studied [1]. However, when faced with high-efficiency, large-scale task requirements, a single AUV cannot meet the requirements. A new approach for resolving intricate marine tasks is offered using multi-AUV systems [2]. Some scholars have recently shown interest in consensus control [3], formation control [4,5], flocking control [6], and containment control [7] of multi-agent systems (MASs). The primary algorithms utilized for multi-AUV formation control are the leader-follower [8], behavior-based [9], and virtual structure [10]. The behavior-based approach allows for the functional diversification of multi-AUV formation, but with poor formation stability [9]. The virtual structure approach offers good stability but imposes a heavy burden on computation and communication [10]. The leader-follower approach operates on the control principle of designating a single AUV as the leader AUV, while assigning the remaining AUVs as the follower AUVs [8]. The motion and attitude of the leader AUV are referenced to calculate the speed and direction of the follower AUVs so that multiple AUVs can sail in formation [8]. The structure of the leader-follower formation algorithm is straightforward and effortless to execute [1].

The AUV relies heavily on the technical foundation provided by the controller's design. In the past decades, a variety of control methods have been presented by scholars, such as PID [11], backstepping (BS) [12], sliding mode control (SMC) [13], and model predictive

control (MPC) [14]. PID is a simple, low-complexity control method; however, accurate control can only be provided in the case of linear models and constant disturbances [11]. Backstepping control is an effective method for controlling nonlinear systems; however, as the order of a system increases, so does its computational complexity [12]. SMC is robust to uncertain models and time-varying parameters. However, SMC suffers from inaccurate control with a low degree of precision, excessive energy usage, and a high level of power consumption [13]. In addition, the above control methods are challenging to manage input and state constraints. In the controller design phase, the constraints of the system are ignored in the above control methods, which leads to poor control performance to a certain extent [14].

MPC uses the current state information of an agent to obtain its predictive state information, which is a closed-loop optimal control strategy. Multiple uncertainties and state constraints in multi-AUV systems can be handled using MPC [15]. MPC aims to tackle constrained optimization problems based on rolling optimization and feedback correction. Moreover, regardless of whether the controlled object is a linear model or a nonlinear model, the predictive model can be combined with the controlled object to achieve a more accurate control. MPC was applied to track the trajectory of unmanned vehicles by Yu et al. [16]. An MPC strategy was used to obtain the current control action online through solving predictive horizon open-loop optimal control [17]. A multi-objective MPC was developed to address the problem of path-following for an AUV [18]. An MPC strategy was presented to address the problem of trajectory tracking [19]. In [20], a Laguerre function-based adaptive predictive control was developed to address the challenge of trajectory tracking for AUVs operating in intricate underwater environments. Simultaneously, the real-time performance and tracking accuracy of the AUV system were improved. A target-tracking approach for AUVs was presented in [21], which utilized an MPC algorithm to account for dynamic behavior, allowing the accurate tracking of dynamic targets and trajectories. Additionally, MPC was employed in [22] to guarantee the control efficacy for linear systems that experience additive perturbations as well as multiple constraints.

The multi-AUV formation encounters various obstacles, such as buoys, reefs, and piers, while sailing. To address the challenge of obstacle avoidance, artificial potential field (APF) [23], MPC [24], and online optimal control method [25] have been developed by researchers. APF suffers from two key issues: goal non-reachable with obstacle nearby (GNWON) and jitter. Online optimal control requires a large amount of computation when the formation size is substantial, leading to a reduction in real-time performance [26]. In [27], the assumed prediction information of a neighbor agent was used to avoid collision. Under the constraints of robot dynamics and obstacle avoidance, a planner based on MPC was designed in [28]. A compatibility constraint was redefined in [29], which limits the deviation between the assumed and actual predicted states of local optimization. The model predictive control of AUV was studied in [30], and an integrated tracking control algorithm that included AUV dynamic path planning was developed. In [31], a dynamic path planning and trajectory tracking algorithm for autonomous satellites was proposed. Furthermore, a finite-horizon MPC strategy was presented. In [32], a framework of path planning was proposed for autonomous vehicles. In [33], an improved particle swarm optimization (IPSO)-based MPC was proposed to address the challenge of path planning.

The significant computational requirement is a disadvantage of MPC. The ET mechanism can effectively decrease computational load [34,35]. Therefore, it is advantageous to integrate the ET mechanism with MPC. It can lower the computational cost while retaining the features of MPC because the controller only updates when events are triggered. The EMPC for multi-vehicle systems was proposed in [36], and the ET mechanism was used to lower the computational load of MPC.

The majority of prior research on multi-agent systems predominantly focused on linear systems [37], as evident from the aforementioned studies, whereas an AUV is a typical nonlinear system. The primary focus of many studies have been on multi-agent systems like UAVs and unmanned vehicles. However, research on the AUV system has been limited

due to the heightened complexity of the underwater environment in comparison to air and land environments.

Motivated by these existing research results and issues, a model predictive control method based on an event-triggered mechanism (EMPC) is proposed for multi-AUV formation in multi-obstacle underwater environments. The relative motion model of the multi-AUV formation is established according to the leader-follower formation control method. A compatible constrained MPC is proposed to plan the obstacle avoidance path of the multi-AUV formation so that the formation can avoid obstacles and reach the target point smoothly. The control problem of the multi-AUV formation is transformed into an optimization problem with input constraints and state constraints through MPC. The next optimal input is calculated according to the current state of the AUV and the desired trajectory, enabling the AUV to track the desired reference path accurately. In addition, an event-triggered mechanism based on the predicted and actual state values of the AUV is established, which can greatly reduce the calculation amount for solving optimization problems. The contributions of this paper are described as follows:

(1) The norm-form compatibility constraint is proposed to address the issue of convergence for multi-AUV formation, that is, the uncertainty deviation between the actual and assumed trajectories of the AUV.
(2) Since MPC has multiple constraints, the constraints of the AUV are embedded into the optimization of MPC, and the speed jump of multi-AUV formation systems can be avoided.
(3) Combining event-triggered mechanisms and MPC, an EMPC strategy is designed to handle multiple constraints and reduce the computational burden of the multi-AUV system.

The remainder of this paper is organized as follows: The preliminaries are introduced in Section 2. In Section 3, the EMPC for multi-AUV systems considering obstacle avoidance is developed. Section 4 presents the main results to demonstrate the efficacy of the proposed approach. In Section 5, a simulation is conducted to further confirm the efficacy of the proposed algorithm. Section 6 concludes this paper and outlines future research.

2. Preliminaries

In this paper, an EMPC for multi-AUV systems obstacle avoidance is designed. The structure flow framework of EMPC is shown in Figure 1, where N represents the quantity of AUVs. The inputs of EMPC are derived from the information detected by the sensor. Then, multi-AUV formation generation, obstacle avoidance, and formation maintenance are realized using actuators. The notations and problem statement are presented in this section.

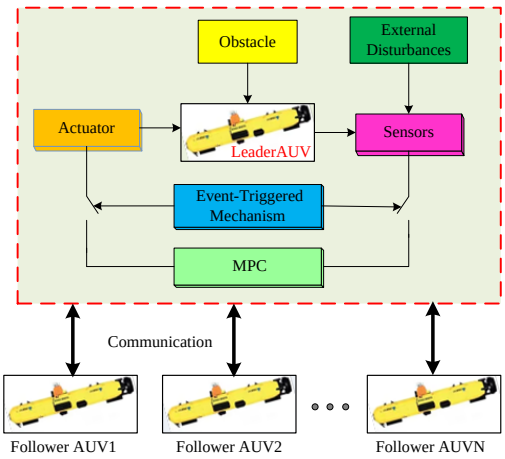

Figure 1. The multi-AUV system architecture based on EMPC.

2.1. Notations

The following notations are adopted in this paper. The Euclidean norm is represented by $||\cdot||$. $||\boldsymbol{\eta}(t)||_B$ represents the norm of $\boldsymbol{\eta}(t)$, weighted by B, where B is a positive definite matrix. The real space of $n \times n$ dimensional matrix is denoted as $\Re^{n\times n}$. $\lambda_{\min}(\cdot)$ and $\lambda_{\max}(\cdot)$ represent the minimum and the maximum of matrix eigenvalues, respectively.

2.2. The Model of Multi-AUV System

The establishment of the inertial coordinate $(X-Y-Z)$ and the body-fixed coordinate $(x_0-y_0-z_0)$ are illustrated in Figure 2. $\boldsymbol{\eta}_i(t) = [\mathbf{p}_i(t), \boldsymbol{\varphi}_i(t)]^T$ is the state of the $AUVi$, where $i \in N$ is the number of AUVs, $\mathbf{p}_i(t) = [x_i(t), y_i(t), z_i(t)]$, $\boldsymbol{\varphi}_i(t)$ is the position and orientation of the $AUVi$. The kinematic equation of the AUV is as follows [38].

$$\dot{\boldsymbol{\eta}} = f(\boldsymbol{\eta}(t), \mathbf{u}(t)) = \begin{bmatrix} \cos\varphi & -\sin\varphi & 0 & 0 \\ \sin\varphi & \cos\varphi & 0 & 0 \\ 0 & 0 & 1 & 0 \\ 0 & 0 & 0 & 1 \end{bmatrix} \mathbf{u}(t) \tag{1}$$

where $f(\cdot)$ is the continuously nonlinear function, and the control input is denoted as $\mathbf{u}(t) = [\mathbf{v},\ r]^T$, where $\mathbf{v} = [u, v, w]^T$. The rate of surge, sway, heave, and yaw are respectively represented by u, v, w, and r.

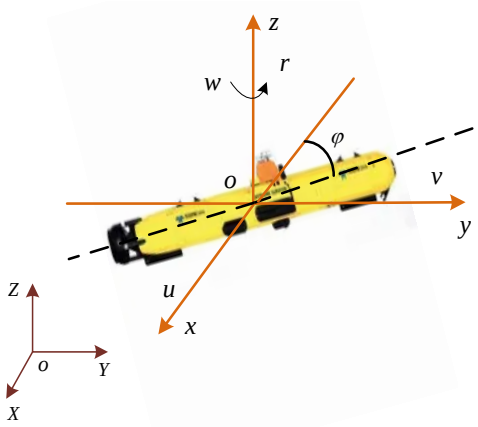

Figure 2. The model of AUV.

Let $\eta_i^d(t)$ be the desired state, $\varphi_i^d(t)$ be the desired heading angle, $\eta_i^e(t) = \eta_i - \eta_i^d$ be the state error, and $\varphi_i^e(t) = \varphi_i(t) - \varphi_i^d(t)$ be the angle error of the $AUVi$. Note that the multi-AUV system is usually subjected to external disturbances. The multi-AUV system with external interference is represented as

$$\dot{\boldsymbol{\eta}} = f(\boldsymbol{\eta}(t), \mathbf{u}(t)) + \mathbf{C}(t), \quad t \geq t_0 \tag{2}$$

where the initial instant is denoted as t_0, $\mathbf{C}(t) \in \Re^n$ is a bounded external disturbance, and $||\mathbf{C}(t)|| \leq C_0$, C_0 is a positive constant.

A typical relative motion model for multiple AUV systems is shown in Figure 3. In this scenario, all AUVs possess identical structural and kinematic models. According to the length l_{iL}^d and azimuth φ_{iL}^d of the intended arrangement of multi-AUV systems, the intended location (x_i^d, y_i^d, z_i^d) and orientation φ_i^d of the follower AUV can be determined as (3).

$$\begin{cases} x_i^d(t) = x_L(t) - l_{iL}^d \cos(\varphi_L(t) + \varphi_{iL}^d) \\ y_i^d(t) = y_L(t) - l_{iL}^d \sin(\varphi_L(t) + \varphi_{iL}^d) \\ z_i^d(t) = z_L(t) - z_i(t) \\ \varphi_i^d = \varphi_L \end{cases} \tag{3}$$

where $p_L = [x_L, y_L, z_L]$ is the location of the leader AUV, and φ_L is the heading angle of the leader AUV.

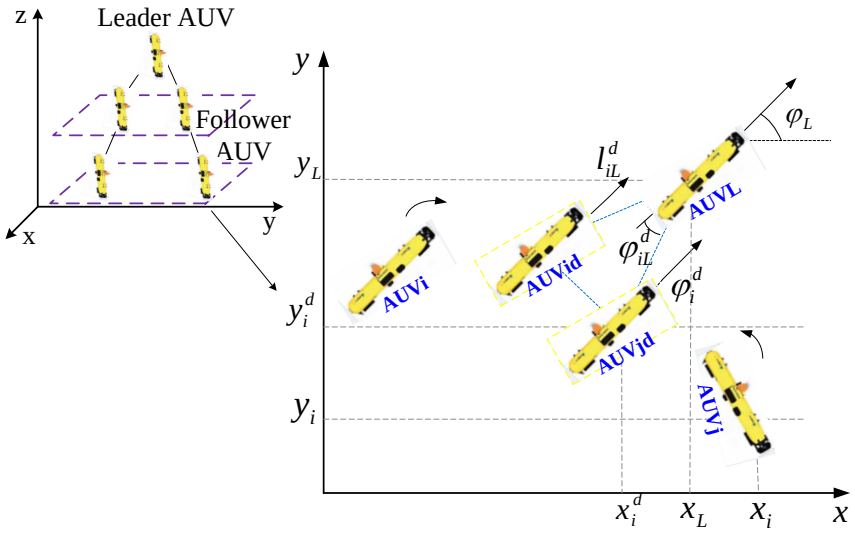

Figure 3. Relative motion model of multi-AUV systems.

2.3. Problem Statement

In order to clearly illustrate the multi-AUV formation obstacle avoidance control, the following assumptions are made.

(1) The AUV can be perfectly located, and the map environment is known.
(2) The starting point, target point, and obstacle position are known before the formation operation.
(3) The multi-AUV formation is achieved without communication delay, packet loss, mechanical failure, or sensor noise.

To ensure the generation, collision, and obstacle avoidance of multi-AUV systems, control objectives are established as follows:

Formation generation:

$$\begin{aligned} \lim_{t\to\infty}(p_L(t) - p_i(t)) = l_{iL}^d,\ \varphi_i(t) = \varphi_L(t) \\ \lim_{t\to\infty}(p_j(t) - p_i(t)) = d_{ij},\ j \in N_i \end{aligned} \tag{4}$$

Collision avoidance of multi-AUV systems:

$$\|p_j(t) - p_i(t)\| \geq R_o,\ j \in N_v \backslash i \tag{5}$$

Obstacle avoidance of multi-AUV systems:

$$\|p_i(t) - p_o\| \geq R_o,\ \ o \in N_o \tag{6}$$

where d_{ij} is the desired distance between the follower $AUVi$ and $AUVj$, p_o denotes the position of an obstacle, R_o is the safe distance between the AUV and an obstacle, N_o is the number of obstacles, and N_i is the neighbor set of the $AUVi$. In addition, for the multi-AUV system, only obstacles with distances less than h away from the $AUVi$ are considered in this paper. Because if an obstacle is too far away from the AUV, the operation of the multi-AUV formation will not be affected. There is

$$\| \overline{p}_{io}(s|t_{k+1}) \| = \| \overline{p}_i(s|t_{k+1}) - p_o \| \leq h,\ \ h > 0 \tag{7}$$

where $t_{k+1} \in [t_k,\ t_k + T]$ is the next update time. The relationship between all the time intervals is shown in Figure 4. At each update time, T is the prediction horizon and t_k

is the current instant. The shortest duration between two events is $\inf\{t_{k+1} - t_k\} = \sigma$. $\sup\{t_{k+1} - t_k\} = T$ is the longest period of time that can elapse between two events.

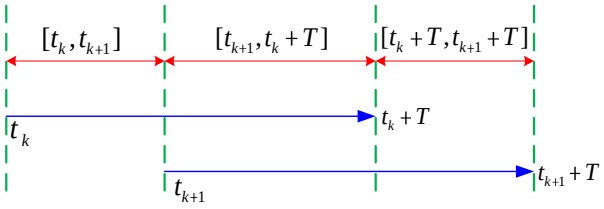

Figure 4. The relationship between time intervals.

Remark 1. *Other neighboring AUVs are regarded as obstacles to avoid collision. Therefore, the safe distances for collision and obstacle avoidance are identical.*

As shown in Figure 5, Ω_i and $\Omega_{\varepsilon i}$ are designed as concentric. The invariant set is denoted by the larger ellipse, and the terminal set is denoted by the smaller ellipse.

$$\Omega_i \triangleq \left\{ p_i^e(t_k) : \|\hat{p}_i^e(s)\|_Z^2 \leq \delta^2 \right\}, \ \Omega_{\varepsilon i} \triangleq \left\{ p_i^e(t_k) : \|\hat{p}_i^e(t_k + T)\|_Z^2 \leq \varepsilon^2 \right\} \tag{8}$$

where $s \in [t_k, t_k + T]$, $\hat{p}_i^e(s|t_k)$ represents the assumed predictive tracking error state trajectory, generated using the assumed predictive input $\hat{u}_i(s|t_k)$ of the *AUVi*. $p_i^{e*}(s|t_k)$ is the optimal predictive tracking error state trajectory, and $\overline{u}_i(s|t_k)$ is the feasible predictive input. Z is the positive definite symmetric matrix, and δ and ε are constants related to the invariant set and the terminal set, respectively. The designed controller is established as follows:

$$\hat{u}_i(s|t_{k+1}) = \begin{cases} u_i^*(s|t_k), & s \in [t_{k+1}, t_k + T], \\ -K_i(\hat{p}_i^{e*}(s|t_k)), & s \in [t_k + T, t_{k+1} + T]. \end{cases} \tag{9}$$

If the actual tracking error state trajectory of the follower *AUVi* is outside the invariant set Ω_i, that is, $P_i^e(t_k) \notin \Omega_i$, the control input is $u_i^*(s|t_k)$. If the actual tracking error state trajectory of the follower *AUVi* is inside the invariant set Ω_i, that is, $P_i^e(t_k) \in \Omega_i$, the control input is $-K_i(\hat{p}_i^{e*}(s|t_k))$.

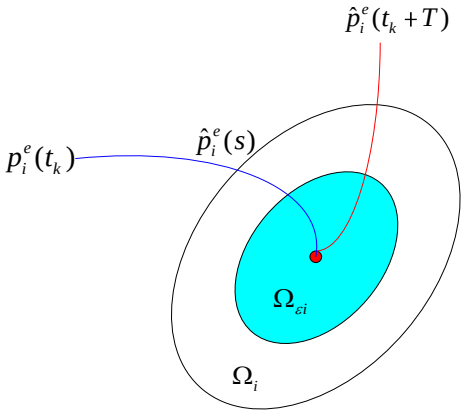

Figure 5. The invariant set Ω_i and terminal set $\Omega_{\varepsilon i}$.

Assumption 1. *$v_i(t)$ is bounded by a, that is, $|v_i(t)| \leq a$, wherea is the upper bound of the linear velocity of the AUVi. r is bounded by $\overline{r}$, and $\overline{r}$ is the upper bound of the angular velocity of the AUV.*

Assumption 2. *According to [36], the nonlinear function $f(\eta_i(t), u_i(t))$ is for the AUVi. There is the following inequality when the Lipschitz constant $L_f > 0$.*

$$\|f(\eta_1(t), u_1(t)) - f(\eta_2(t), u_2(t))\|_{p_i} \leq L_f \|\eta_1(t) - \eta_2(t)\|_{p_i} \tag{10}$$

Assumption 3. *According to [39], the local convergence condition for the AUVi is*

$$\sum_{i \in N} \left(\dot{g}_i(p_i^e(s|t_k)) + L_i\left(p_i^e(t_k), u_i^e(t_k)\right)\right) \leq 0 \tag{11}$$

Lemma 1. *According to[[40]], if there is a Lipschitz constant $L_f = a$, the system (1) is locally Lipschitz in $\eta_i(t)$with $u_i(t) \in U$.*

Lemma 2. *The deviation of the AUV's trajectory between the actual and optimal states is limited by*

$$\| \eta_i(s) - \eta_i^*(s|t_k) \| \leq \rho(s - t_k) \tag{12}$$

where $s \in [t_k, t_k + T]$, $\rho(\tau) = C_0 s e^{a\tau}$.

Lemma 3. *According to [41], if $\|u_L(t)\| < \alpha/\beta$holds, the ideal control input of the AUV is constructed using $\left|\tilde{v}^d(t)\right|/\tilde{a} + \left|\tilde{r}^d(t)\right|/\tilde{\bar{r}} \leq \gamma$, $\gamma \in (0,1)$ is a constant. The minimum value of γ is*

$$\gamma_{\min} = \max\{\|u_L(t)\|_2\}\frac{\beta}{\alpha}. \tag{13}$$

where $\alpha = \dfrac{\mu a \bar{r}}{\sqrt{a^2 + (\mu \bar{r})^2}}$, $\beta = \|M\|_2$, the control input of the leader AUV is denoted as $u_L(t)$, μ is the offset, and M is a matrix.

3. Design of EMPC for Multi-AUV Systems

There are multiple uncertainties and state constraints in multi-AUV systems. Uncertainties refers to system uncertainty due to the limitations and imperfect models of the AUV, making it impossible for the AUV to fully and accurately predict its own behavior and respond to environmental changes during task execution [42]. In this section, EMPC is designed to control the multi-AUV system. Simultaneously, an ET mechanism is designed to lower the computational burden caused by using MPC. The design of EMPC is mainly presented in this section.

3.1. Methodology

A multi-AUV formation obstacle avoidance control based on event-triggered model predictive control (EMPC) is proposed in this paper. The control structure diagram of the multi-AUV system is shown in Figure 6. Under the control of EMPC, each AUV in the formation converges to the desired state. The key steps are as follows:

(1) A mathematical model of the multi-AUV system is established.
(2) A norm-form compatibility constraint is proposed to address the issues of convergence and obstacle avoidance for multi-AUV systems.
(3) Multiple constraints are embedded in MPC to avoid the speed jump in multi-AUV systems.
(4) An EMPC is designed to handle multiple constraints and minimize the computational workload of multi-AUV systems.
(5) Finally, the feasibility and stability of the system are analyzed.

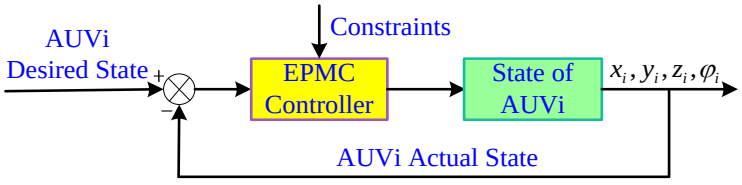

Figure 6. The control structure diagram of the multi-AUV system.

3.2. Optimization Problem

The optimal cost should be considered in MPC, so it is necessary to construct the cost and optimization function of MPC. The cost function of the *AUVi* is

$$J_i(p_i^e(t_k), u_i^e(t_k)) = \int_{t_k}^{t_k+T} L_i(p_i^e(t_k), u_i^e(t_k))ds + g_i(p_i^e(t_k+T)), \tag{14}$$

where

$$L_i(p_i^e(t_k), u_i^e(t_k)) = \| p_i^e(s|t_k) \|_P^2 + \sum_{j\in N_i} \| p_{ij}(s|t_k) \|_Q^2 + \| p_{io}(s|t_k) \|_R^2 + \| u_i^e(s|t_k) \|_S^2, \tag{15}$$

$$g_i(p_i^e(t_k+T)) = \| p_i^e(t_k+T|t_k) \|_Z^2 + \| p_{ij}(t_k+T|t_k) \|_Z^2 + \| p_{io}(t_k+T|t_k) \|_Z^2, \tag{16}$$

where $L_i(p_i^e(t_k), u_i^e(t_k))$ is the stage cost function, $\| p_i^e(s|t_k) \|_P^2$ is the position tracking penalty term, $\| p_{ij}(s|t_k) \|_Q^2$ is the position formation penalty term, $\| p_{io}(s|t_k) \|_R^2$ is the obstacle avoidance penalty term, and $\| u_i^e(s|t_k) \|_S^2$ is the velocity tracking penalty term. The terminal cost function is denoted as $g_i(p_i^e(t_k+T))$. P, Q, R, S, and Z are positive definite symmetric matrices.

The optimization of MPC for the *AUVi* is constructed as follows:

$$\min_{u_i(s|t_k)} J_i(p_i^e(t_k), u_i^e(t_k)) \tag{17}$$

$$s.t.\ \eta_i(t_k|t_k) = \eta_i(t_k) \tag{18}$$

$$\dot{\eta}_i(s|t_k) = f(\eta_i(s|t_k), u_i(s|t_k)) \tag{19}$$

$$u_i(s|t_k) \in U_i \tag{20}$$

$$\| p_i^e(s|t_k) \| \le \frac{T\varepsilon}{s-t_k} \tag{21}$$

$$p_i^e(t_k+T|t_k) \in \Omega_{\varepsilon i} \tag{22}$$

$$C_1(\pi_i(s|t_k), \phi_i(t_k), \psi_i(t_k)) \le 0 \tag{23}$$

$$C_2(p_i(s|t_k), \hat{p}_j(s|t_k)) \le 0 \tag{24}$$

$$C_3(p_i(s|t_k), p_o) \le 0 \tag{25}$$

where t_k is an update instant, $s \in [t_k, t_k+T]$. The optimal cost function is expressed as follows:

$$J_i(p_i^{e*}(t_k), u_i^{e*}(t_k)) = \int_{t_k}^{t_k+T} L_i(p_i^{e*}(t_k), u_i^{e*}(t_k))ds + g_i(p_i^{e*}(t_k+T)). \tag{26}$$

3.3. The Event-Triggered Mechanism

To lower the computational load, the ET mechanism is established. The condition for ET is expressed as

$$\| \eta_i(s) - \eta_i^*(s|t_k) \| \ge \rho(\sigma), \tag{27}$$

where $\sigma \in (0, T)$. When Equation (27) is not satisfied, a lower bound of triggering time is obtained as follows:

$$\tilde{t}_{k+1} = \inf_{s\in[t_k,t_k+T]} s : \| \eta_i(s) - \eta_i^*(s|t_k) \| \ge \rho(\sigma) \tag{28}$$

Note that at both t_0 and $t_k + T$, the multi-AUV system is obliged to be triggered at least once. The designed triggering time t_{k+1} is:

$$t_{k+1} = \min\{\tilde{t}_{k+1}, t_k + T\}. \tag{29}$$

Remark 2. *The disparity between adjacent update times in two events is $t_{k+1} - t_k$. Zeno behavior usually exists in the ET mechanism, indicating repeated triggering within a finite time limit. The minimum time between two events is $inf\{t_{k+1} - t_k\} = \sigma$, and the max time between two events is $sup\{t_{k+1} - t_k\} = T$. Hence, the Zeno behavior is naturally avoided in this paper.*

3.4. The Constraints Design

The constraints of multi-AUV systems are designed in this section.

Firstly, let

$$\phi_{ij}(t_k) = \min_{j \in N \backslash i} \left\{ \frac{\| \hat{p}_j(s|t_k) - \hat{p}_i(s|t_k) \| - R_o}{2} \right\}, \ s \in [t_k, t_k + T]. \tag{30}$$

The limit on collision avoidance $\phi_i(t_k)$ is denoted as

$$\phi_i(t_k) = \min_{j \in N \backslash i} \{\phi_{ij}(t_k)\}. \tag{31}$$

The bound of tracking and formation $\psi_i(t_k)$ is [36]:

$$\psi_i(t_k) = \frac{\vartheta \left(\|\eta_i^e(t_k)\|_P^2 + \sum_{j \in N_i} \|p_{ij}(t_k)\|_Q^2 \right)}{(T - T_p) \sum_{j \in N_i} \lambda_{\max}(Q)(2e_{ij}(k) + 3\phi_{ij}(k))}, \tag{32}$$

where

$$e_{ij}(t_k) = \max_{s \in [t_{k+1}, t_k + T]} \| \hat{p}_j(s|t_k) - \hat{p}_i(s|t_k) + d_{ji} \|, \tag{33}$$

where the sampling period is denoted as T_p, and $\vartheta \in [0, 1)$ is a constant. The uncertain deviation between the assumed and actual trajectories of the $AUVi$ $\pi_i(s|t_k)$ is introduced.

$$\| \pi_i(s|t_k) \| \leq \min\{\phi_i(t_k), \psi_i(t_k)\}, \tag{34}$$

where $\pi_i(s|t_k) = \hat{p}_i(s|t_k) - p_i(s|t_k)$.

The compatibility constraint is constructed as

$$C_1(\pi_i(s|t_k), \phi_i(t_k), \psi_i(t_k)) = \| \pi_i(s|t_k) \| - \min\{\phi_i(t_k), \psi_i(t_k)\}, \tag{35}$$

and the collision avoidance constraint for the $AUVi$ is

$$\| p_j(s|t_k) - p_i(s|t_k) \| \geq R_o. \tag{36}$$

Considering the constraint (34), there is

$$\begin{aligned} \| p_j(s|t_k) - p_i(s|t_k) \| &= \| \hat{p}_j(s|t_k) - p_i(s|t_k) - \pi_j(s|t_k) \| \\ &\geq \| p_j(s|t_k) - p_i(s|t_k) \| - \phi_{ij}(t_k) \end{aligned}. \tag{37}$$

According to inequalities (36) and (37), we have

$$\| \hat{p}_j(s|t_k) - p_i(s|t_k) \| \geq R_o + \phi_{ij}(t_k), \ \ j \in N \backslash i \tag{38}$$

The designed constraint of collision avoidance is

$$C_2(p_i(s|t_k), \hat{p}_j(s|t_k)) = R_o + \phi_{ij}(t_k) - \| \hat{p}_j(s|t_k) - p_i(s|t_k) \|. \tag{39}$$

According to (6), we have

$$\| p_i(s|t_k) - p_o \| \geq R_o. \tag{40}$$

The obstacle avoidance constraint is

$$C_3(p_i(s|t_k), p_o) = R_o - \| p_i(s|t_k) - p_o \|. \tag{41}$$

3.5. EMPC Design

The EMPC strategy is proposed in this section to accomplish control objectives (4)–(6). To reduce the computational burden, the ET mechanism is integrated into MPC, which is shown in Algorithm 1. The first step is to choose the parameters. Each AUV maintains its communication. The optimal control sequence and the trajectory of the tracking error state are calculated prior to the entry of the tracking error state into Ω_i. The terminal controller is activated to drive the tracking error state to enter $\Omega_{\varepsilon i}$. The ET strategy is developed based on the variation between the actual trajectory and the optimal prediction. The ET condition determines the next update time.

Algorithm 1. Algorithm to design EPMC scheme.

Input: The initial and target state of AUVs; the parameters P, Q, R, S, Z, ϑ, $\hat{k}_1$ and $\hat{k}_2$.
Output:
Begin:

1. Step 1: At t_0, according to $\hat{p}_i(s|t_0) = p_i(t_0)$, the $AUVi$ sends $\hat{p}_i(s|t_0)$ to the $AUVj$, and receives $\hat{p}_j(s\big|t_0)$ from the $AUVj$.
2. Step 2: At sample instant t_p, compute $\phi_{ij}(t_k)$, $\phi_i(t_k)$, $\psi_i(t_k)$.
3. Step 3: At t_k, if $p_i^e(t_k) \notin \Omega_i$, the optimization problem (13a)-(13i) is solved to obtain $u_i^*(s)$ and $\hat{p}_i^{e*}(s)$, $s \in [t_k, t_k + T]$. If $p_i^e(t_k) \in \Omega_i$, switch to the terminal controller, $\hat{u}_i(s\big|t_k) = -K_i(\hat{p}_i^e(t_k))$.
4. Step 4: $t_{k+1} = \min\{\hat{t}_{k+1}, t_k + T\}$ is given as:
   (a) If (27) is satisfied, then $t_{k+1} = \hat{t}_{k+1} = \inf_{s\in[t_k, t_k+T]} s : ||\eta_i(s) - \eta_i^*(s|t_k)|| \geq \rho(\sigma)$.
   (b) Or else, $t_{k+1} = t_k + T$.
5. Step 5: Set $t_k = t_{k+1}$, and proceed to Step 1.

End

Remark 3. *In Algorithm 1, the selection of T is necessary. Whereas the computational load will be heavy if T is too long, the control effect will be worse if T is too short. Selecting a suitable sampling period T_p is crucial. If T_p is too large, it will lead to a suboptimal control effect. If T_p is too small, the computational burden will be heavy.*

4. Main Results

In this section, we present the proposed analysis of feasibility and stability.

4.1. Feasibility Analysis

The feasibility analysis is proposed in this part.

Theorem 1. *Set*

$$\Omega_{\varepsilon i} = \left\{ p_i^{e*}(t_k + T\big|t_k) : \| p_i^{e*}(t_k + T|t_k) \|^2 \leq \varepsilon^2 \right\} \tag{42}$$

as the terminal region.

If Equations (17)–(25) are solved at t_k, they will be feasible at t_{k+1}. For all $t_k > 0$, the $AUVi$ neither collides with $AUVj$ nor with obstacles, and

$$C_0 \leq \frac{e^{-aT}}{\sigma}(\delta - \varepsilon),\ \sigma \geq \frac{1}{\hat{k}} \ln \frac{\delta}{\varepsilon},\ \varpi\delta \leq \varepsilon < \delta, \tag{43}$$

where $\delta = \frac{a(1-\gamma)}{\sqrt{\hat{k}_1^2 + \hat{k}_2^2}}$, $\hat{k}_1$ and $\hat{k}_2$ are the parameters for feedback gain values, $\hat{k} = \min\left\{\hat{k}_1, \hat{k}_2\right\}$, $\varpi = \max\left\{\frac{T-\sigma}{T}, \frac{1}{T\hat{k}}\right\}$ with $T\hat{k} > 1$.

The detailed proof is reported in Appendix A.

4.2. Stability Analysis

Theorem 2. *In the multi-AUV system, the EMPC strategy with function (14) is considered. If the following inequality holds, the multi-AUV system is stable.*

$$\begin{aligned}&\sigma(\lambda_{\min}(P)\varepsilon^2 + R_o^2) - \frac{\lambda_{\max}(P)C_0^2\sigma^2}{2a}(e^{2aT} - e^{2a\sigma}) - 2R\lambda_{\max}(Z)C_0\sigma e^{aT} - h^2(\lambda_{\max}(R)T + \lambda_{\max}(Z)) \\ &- \frac{2\lambda_{\max}(P)C_0\sigma\varepsilon}{\sqrt{2a}}\left(\frac{T^2}{\sigma} - T\right)^{\frac{1}{2}}(e^{2aT} - e^{2a\sigma})^{\frac{1}{2}} > 0\end{aligned} \tag{44}$$

The detailed proof is reported in Appendix A.

5. Simulation

In this section, the multi-AUV formation control in complex obstacle environments is simulated directly using a MATLAB R2019a software platform, without using Simulink or other toolboxes.

The following aspects are verified through simulation.

(1) Whether the multi-AUV formation can be generated, and its desired reference path can be accurately tracked, under the control of EMPC. Compared with MPC and the backstepping control method, the advantages of the proposed algorithm are verified.
(2) Can obstacle avoidance and collision avoidance be satisfied by the proposed algorithm?
(3) Can the ET mechanism effectively reduce the computational load?

5.1. Simulation Results in 3D Obstacle-Free Environments

Firstly, the efficacy of the suggested algorithm is validated in a 3D obstacle-free environment with a formation of three AUVs, that is, $N = 3$. The multi-AUV formation forms an equilateral triangle that has a side length of 4 m, that is, the length $l_{iL}^d = 4$ m, and azimuth $\varphi_{iL}^d = \pi/6$. AUV0 is the leader AUV, and AUV1,2 are follower AUVs. Let $a = 2$ m/s, $\bar{r} = 1$ rad/s, $T = 2$ s, and $T_p = 0.1$ s. The parameters of BS are set as $k_{xy} = 3$ and $k_z = k_\varphi = 6$. Table 1 displays the simulation parameters.

Table 1. Simulation parameters.

Parameters	Value	Parameters	Value
ϑ	0.99	ε	0.35
$\hat{k}_1$	0.88	μ	0.12
$\hat{k}_2$	1.08	P	$diag\{0.5, 0.5, 0.5\}$
C_O	0.02	Q	$diag\{0.04, 0.04, 0.04\}$
σ	2×10^{-3}	R	$diag\{0.02, 0.02, 0.02\}$
R_o	2	S	$diag\{0.7, 0.7, 0.7\}$
γ	0.89	Z	$diag\{0.5, 0.5, 0.5\}$
δ	0.75		

The starting condition of each AUV is as follows: $\eta_0(t_0) = [-2, 5, 2, 0]^T$, $\eta_1(t_0) = [-3, 4, 1, 0]^T$, $\eta_2(t_0) = [2, 3, 0, 0]^T$. The target state of AUV0 is set as $(20, 20, 20, 0)$. The desired trajectory of AUV0 is as follows: $x_d(t) = t$, $y_d(t) = t$, $z_d(t) = t$, $\varphi_d(t) = \pi/4$. The reference speed is as follows: $u_d(t) = \sqrt{2}$ m/s, $v_d(t) = 0$ m/s, $w_d(t) = 1$ m/s, $r_d(t) = 0$ rad/s.

The trajectory of each AUV using the MPC, EMPC, and backstepping methods is shown in Figure 7. Figure 7a illustrates that under the control of EMPC, every AUV has the capability to track the desired trajectory in a stable manner and effectively reach the intended target location. According to Figure 7b, MPC requires a significant amount of time for each AUV to follow the desired trajectory, about 4 s. According to Figures 8–10, under the control of EMPC and MPC, the speed of each AUV does not exceed the limit.

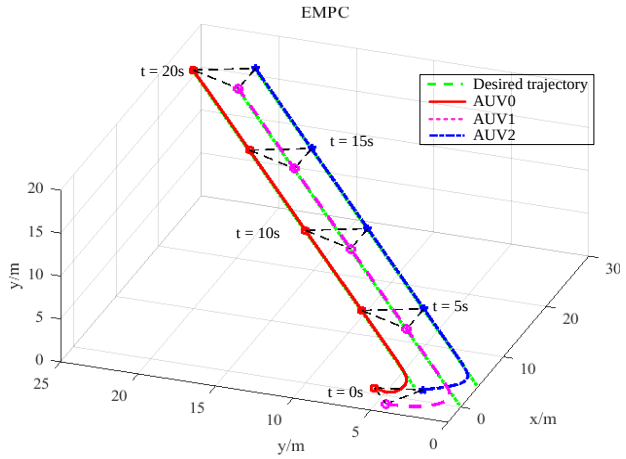

(**a**)

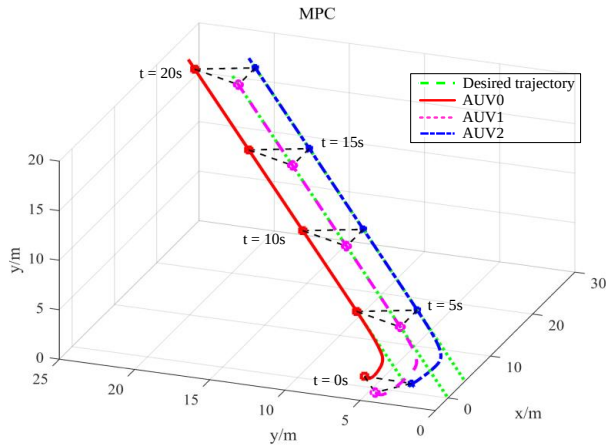

(**b**)

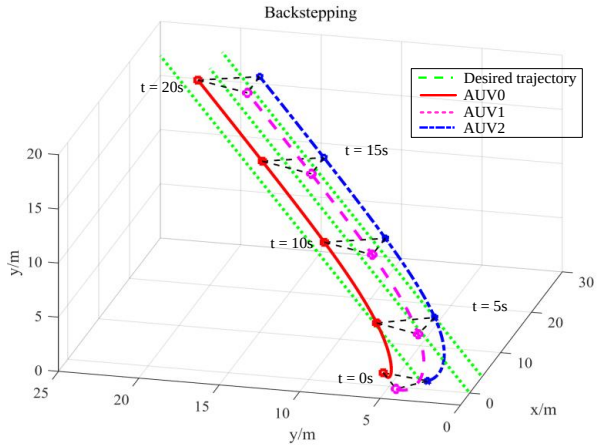

(**c**)

Figure 7. (**a**)**.** Simulation results of linear trajectory tracking control in 3D under EMPC. (**b**). Simulation results of linear trajectory tracking control in 3D under MPC. (**c**). Simulation results of linear trajectory tracking control in 3D under backstepping control.

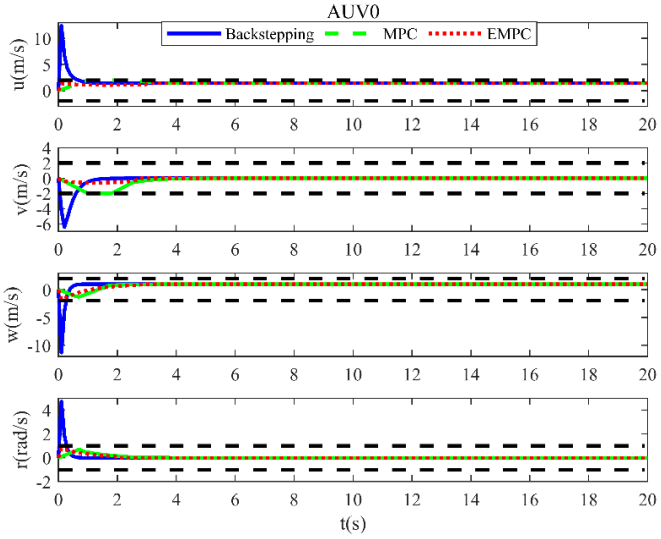

Figure 8. Speed of leader AUV0 of linear trajectory tracking.

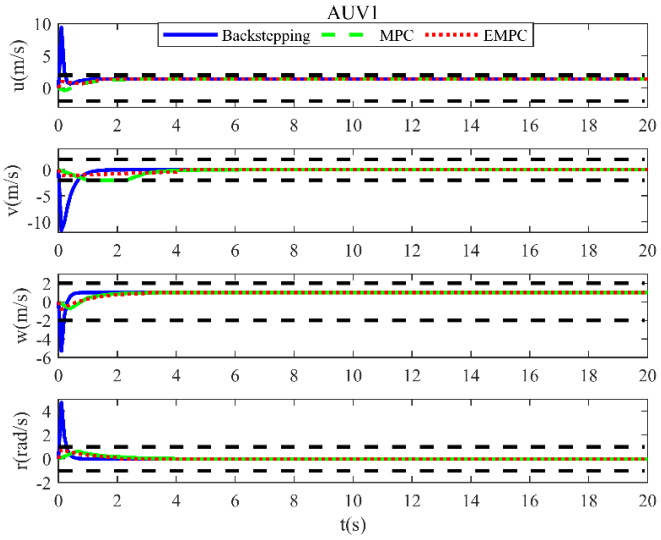

Figure 9. Speed of follower AUV1 of linear trajectory tracking.

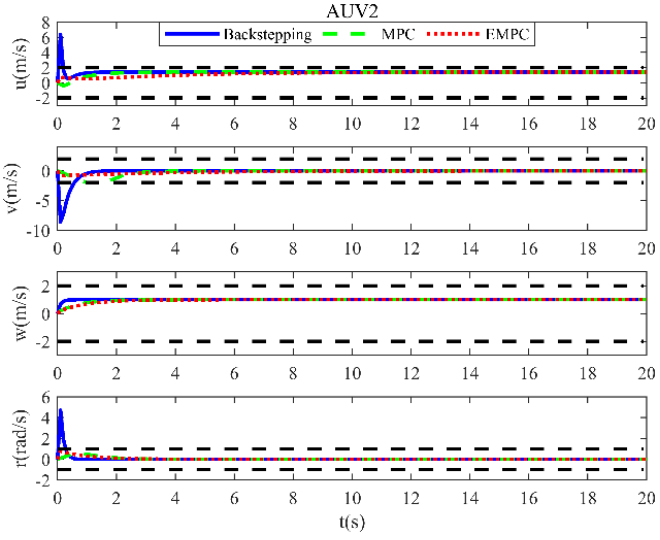

Figure 10. Speed of follower AUV2 of linear trajectory tracking.

According to Figures 8–10, under backstepping control, both the linear speed and the angular speed exceed the limit (the speed limit is indicated by the black dotted line). However, in practical applications, each AUV is given a corresponding speed limit. Therefore, when the speed of the AUV exceeds the limit, the maximum speed limit is used as the control input to obtain the track trajectory results, as depicted in Figure 7c. It is evident from Figure 7c that under backstepping control, each AUV fails to track the desired path and does not reach the target point.

Considering the large amount of computation required when MPC solves optimization problems, an event-triggered mechanism is proposed in this paper. Traditional MPC controllers are time-triggered, and the problem of optimization should be solved at each time step, i.e., each sampling will trigger a controller update. The triggering instants of each follower AUV in obstacle-free environments is shown in Figure 11. The number of triggers rises notably at the beginning, due to state errors in the initial formation generation stage.

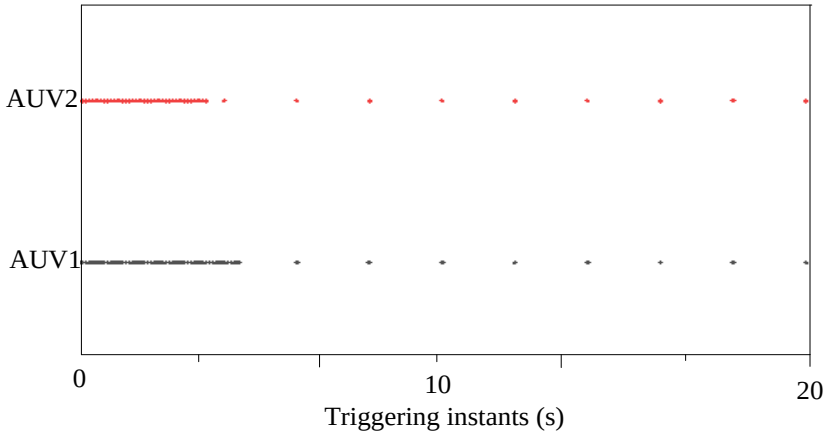

Figure 11. The triggering instants of each follower AUV in obstacle-free environments.

The complete simulation duration for implementing the MPC approach is 156.58 s, which is significantly longer than the 34.69 s required for utilizing the suggested EMPC method. The comparison outcomes for the overall distance for each AUV under the control of the EMPC and the MPC strategy are shown in Figure 12. According to Figure 12, the total distance of each AUV with the EMPC strategy is less than that with the MPC strategy.

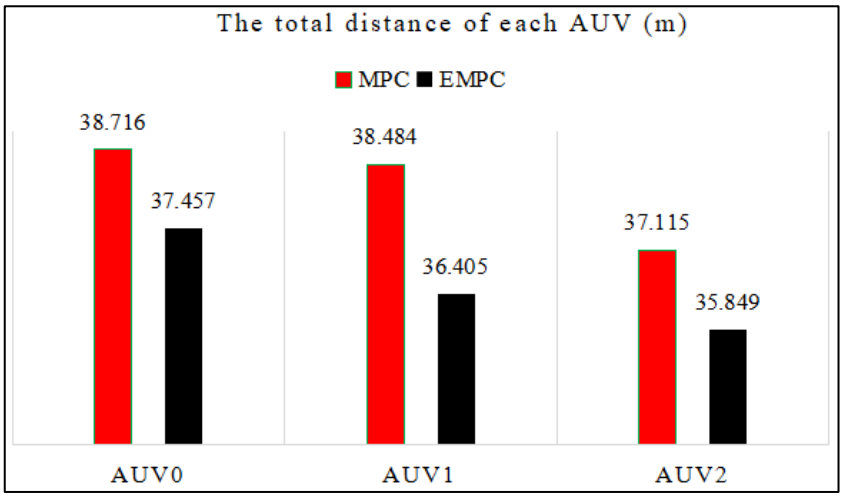

Figure 12. The total distance of each AUV under EMPC/MPC in obstacle-free environments.

5.2. Simulation Results in 3D Obstacle Environments

Simulation experiments are adopted to validate obstacle avoidance as well as collision ability. Note that the backstepping method has no corresponding constraints, so it does not have the ability to avoid obstacles and collisions. The initial condition of each AUV is $\eta_0(t_0) = [1, 1, 5, 0]^T$, $\eta_1(t_0) = [1, 10, -7, 0]^T$, $\eta_2(t_0) = [1, -7, -2, 0]^T$. The location parameters of each obstacle are shown in Table 2, where D represents the diameter, L is the length, W is the width, and h is the height of the cylinder.

Table 2. The location parameters of each obstacle.

Obstacles	Position (m)	Diameter/Side Length (m)
1	(10, 10, 19)	D = 6
2	(20, 23, 25)	D = 5
3	(40, 46, −85)	D = 3, h = 85
4	(40,60, −40)	D = 6, h = 85
5	(37,22, −40)	L = 12.5, w = 12.5, h = 45

It can be seen from Figures 13 and 14 that under the proposed constraints, the five obstacles in the figure can be successfully avoided under the EMPC and MPC strategies, and the multi-AUV formation operation can be maintained. The speed of each AUV under the control of EMPC/MPC in complex obstacle environments is shown in Figures 15–17. Compared with the MPC strategy, the formation convergence rate is faster when the EMPC strategy is adopted. In addition, each AUV can quickly track the reference trajectory under EMPC control after avoiding obstacles. Figures 15–17 illustrate that the speed changes in the formation generation phase as well as the obstacle avoidance phase, but the speed of each AUV is within the constraint range.

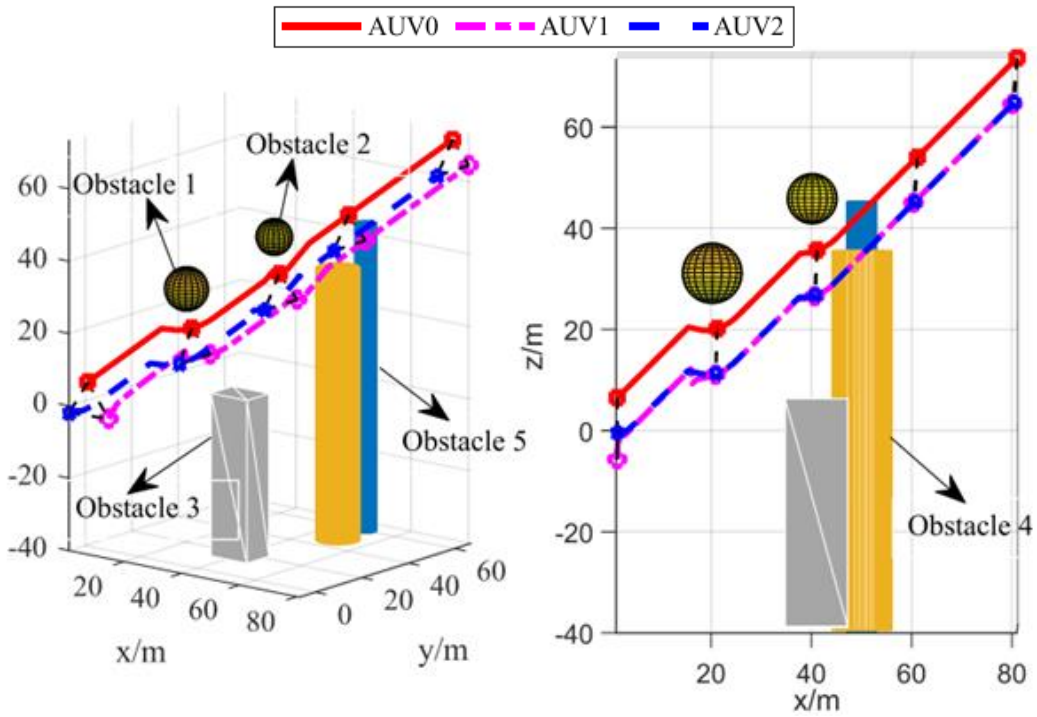

Figure 13. The EMPC-based trajectory in complex obstacle environments.

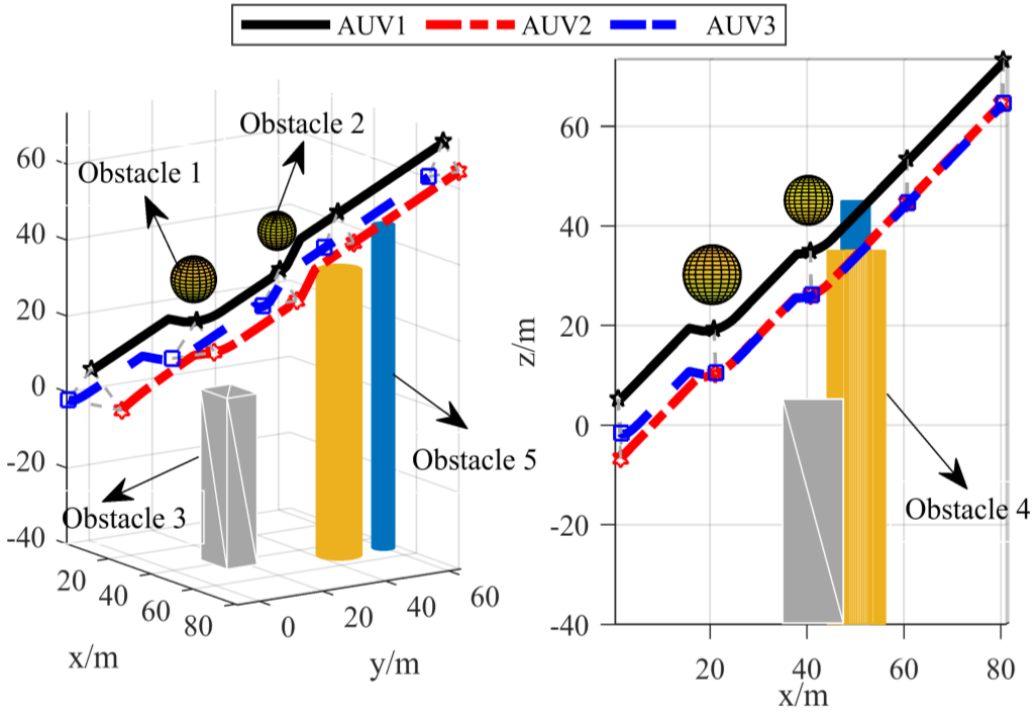

Figure 14. The MPC-based trajectory in complex obstacle environments.

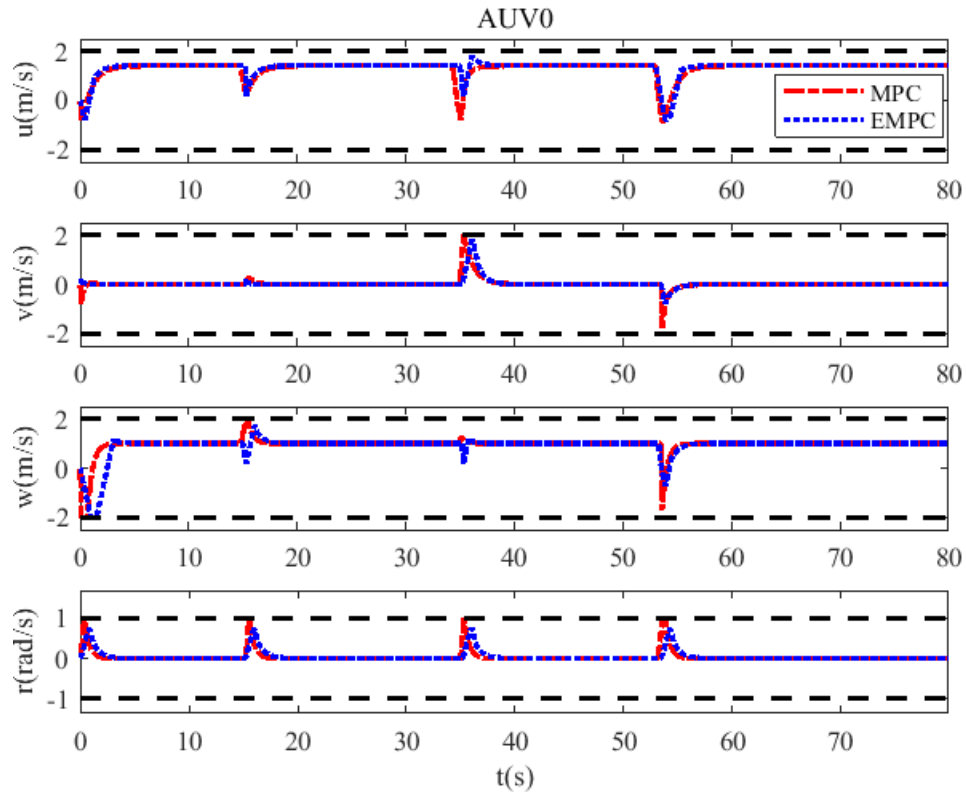

Figure 15. Speed of AUV0 in complex obstacle environments.

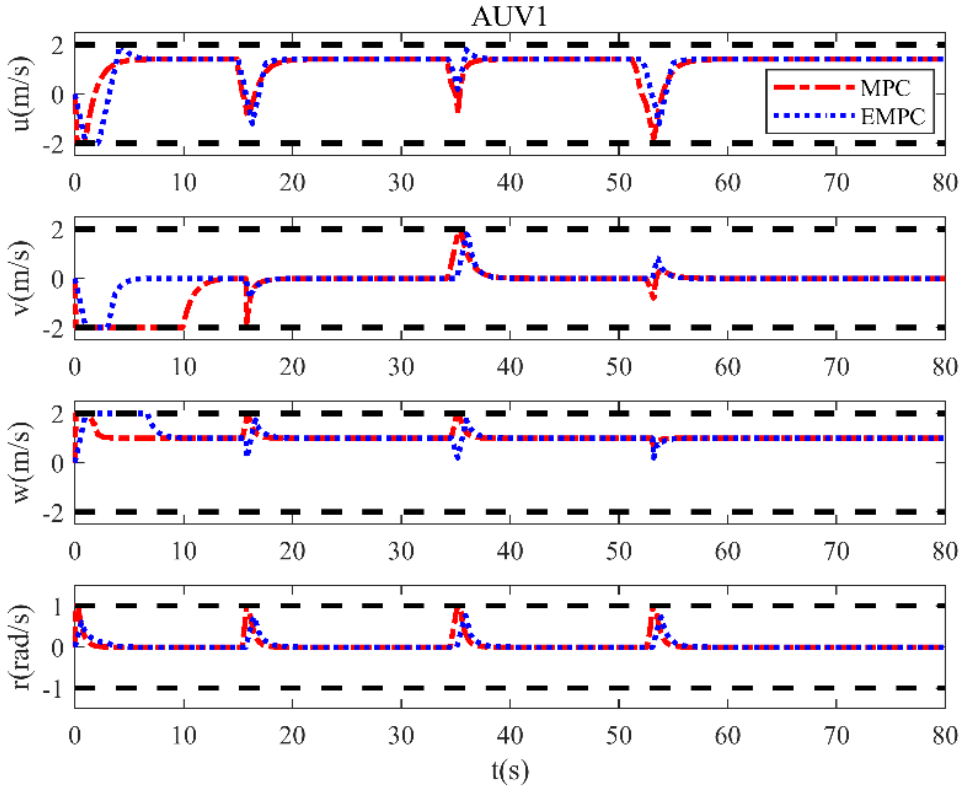

Figure 16. Speed of AUV1 in complex obstacle environments.

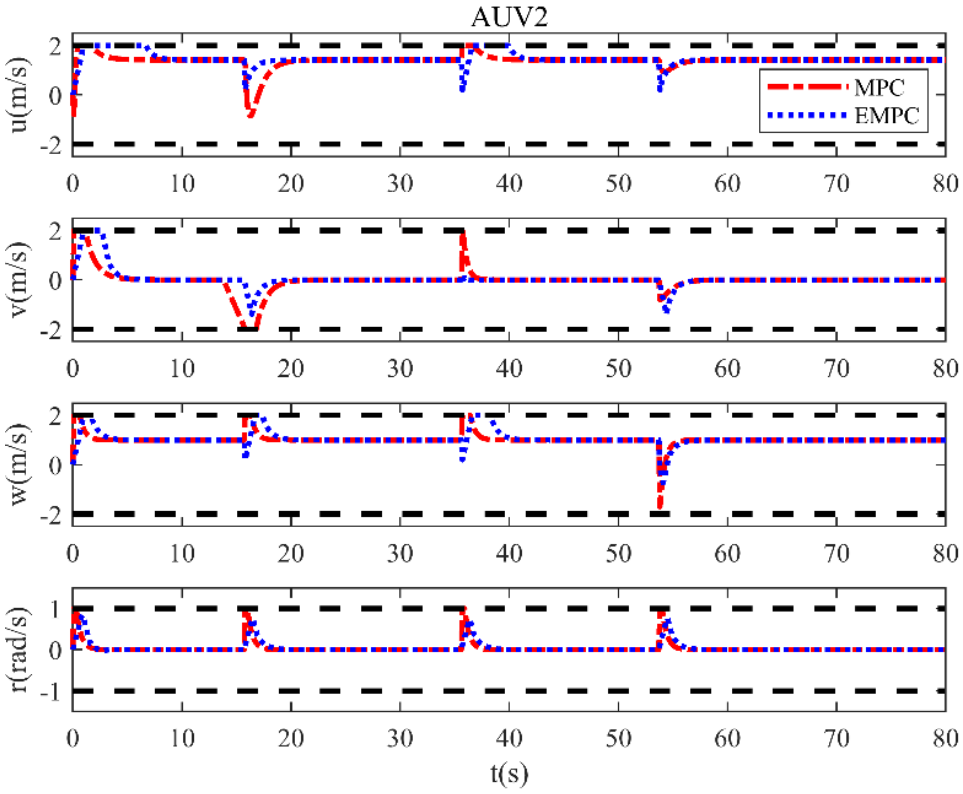

Figure 17. Speed of AUV2 in complex obstacle environments.

The triggering moments of each follower AUV are displayed in Figure 18. There are state errors in the initial formation generation phase and the obstacle avoidance phase. Therefore, the number of triggers increases significantly at the initial time and when obsta-

cles are encountered. The entire simulation duration for implementing the MPC approach is 156.58 s, and the duration for using the EMPC strategy is 45.32 s. The comparison results of the total distance for each AUV under the control of the EMPC and the MPC strategies are shown in Figure 19. According to Figure 19, the total distance of each AUV with the EMPC strategy is less than that with the MPC strategy.

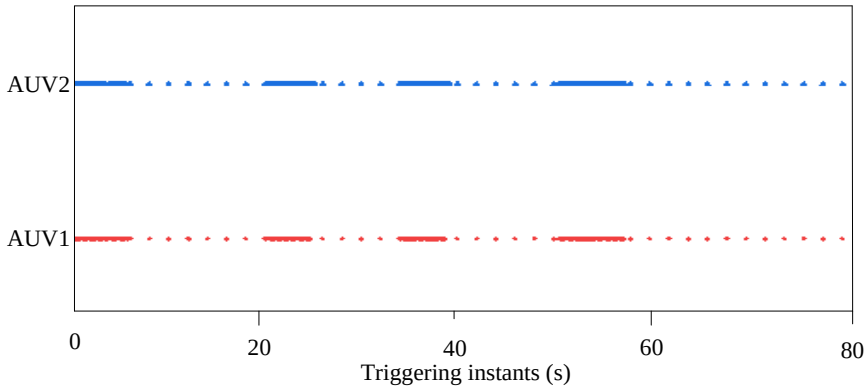

Figure 18. The triggering instants of the follower AUV in complex obstacle environments.

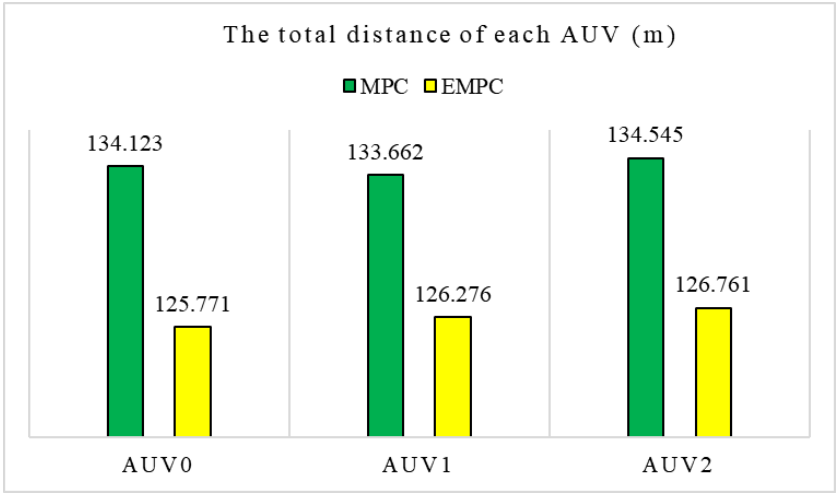

Figure 19. The total distance of each follower AUV under EMPC/MPC in complex obstacle environments.

Evidently, when the ET mechanism is adopted, the number of each follower AUV triggering instant is significantly reduced. When the EMPC strategy is adopted, the time consumed by the system and the total distance of each AUV are less than those of the MPC strategy, which indicates that the event-triggered mechanism proposed in this paper can effectively save computational resources.

6. Conclusions

An EMPC strategy for tracking and obstacle avoidance in a multi-AUV formation system with bounded interference is presented in this paper. The uncertain deviation of each AUV is bounded by a compatibility constraint, which guarantees the convergence of the multi-AUV formation. In addition, avoidance constraints are designed between each AUV and obstacles as well as between each AUV and other AUVs, to ensure that each AUV can avoid obstacles and collisions. The feasibility of EMPC and the stability of the system are guaranteed. Since MPC has multiple constraints, the problem of speed jump can be avoided. The proposed EMPC strategy has been validated through simulation examples, demonstrating its effectiveness and advantages. In addition, MPC presents a heavy computational burden. An event-triggered control mechanism that reduces the communication and computational burden is proposed.

However, most existing studies have focused on static obstacles, and future related work should be aimed at obstacle avoidance control in dynamic obstacle environments as well as the control of heterogeneous systems. In addition, the ocean current environment is not considered in this paper. In the future, obstacle avoidance in the ocean current environment will be further studied. In addition, we will focus on comparing our work with state-of-the-art solutions in subsequent research to increase the quality of this paper.

Author Contributions: Conceptualization, L.W.; Methodology, L.W.; Software, L.W.; Validation, H.Z.; Formal analysis, H.Z.; Investigation, H.Z.; Writing—original draft, L.W. Writing—review & editing, X.X.; Supervision, X.X.; Project administration, X.X; Supervision, B.H.; Writing—review & editing, B.H. All authors have read and agreed to the published version of the manuscript.

Funding: This research was sponsored by the Natural Science Foundation of Fujian Province of China 2022J011128, the Shanghai Science and Program of Shanghai Academic/Technology Research Leader (23XD1431000), and the Innovative Talent Training Project of Graduate Students in Shanghai Maritime University of China (2022YBR006).

Conflicts of Interest: The authors declare no conflict of interest.

Nomenclature

The abbreviations used in this paper are described in the following list.

AUV	Autonomous Underwater Vehicle
Multi-AUVs	Multiple Autonomous Underwater Vehicles
MPC	Model Predictive Control
EMPC	Event-Triggered Model Predictive Control
ET	Event-Triggered Mechanism
SMC	Sliding Mode Control
APF	Artificial Potential Field
IAPF	Improved Artificial Potential Field
IPSO	Improved Particle Swarm Optimization
MASs	Multi-Agent Systems

Appendix A

The detailed proof of Theorem 1.

Proof. The constraints (18)–(20) can be held at t_{k+1} if (17)–(25) is solved at t_k. From (27), Assumption 2, and Lemmas 1 and 2, the divergence between the feasible and the optimal tracking error is

$$\begin{aligned} &\| \overline{p}_i^e(s|t_{k+1}) - p_i^{e*}(s|t_k) \| \le \| \overline{\eta}_i(s|t_{k+1}) - \eta_i^*(s|t_k) \| \\ &= \|\eta_i(t_{k+1}) + \textstyle\int_{t_{k+1}}^{s} f_i(\overline{\eta}_i(\tau|t_{k+1}), u_i^*(\tau|t_k))d\tau - \eta_i^*(t_{k+1}|t_k) - \int_{t_{k+1}}^{s} f_i(\eta_i^*(\tau|t_k), u_i^*(\tau|t_k))d\tau\| \\ &\le \rho(\sigma) + a\textstyle\int_{t_{k+1}}^{s} \| \overline{\eta}_i(\tau|t_{k+1}) - \eta_i^*(\tau|t_k) \| d\tau \end{aligned} \tag{A1}$$

where $s \in [t_{k+1}, t_k + T]$. According to the Gronwall–Bellman inequality, there is

$$\| \overline{p}_i^e(s|t_{k+1}) - p_i^{e*}(s|t_k) \| \le \rho(\sigma) e^{a(s-t_{k+1})} \tag{A2}$$

In addition, according to $s = t_k + T$ and $\rho(\sigma) = C_0 \sigma e^{a\sigma}$, there is

$$\| \overline{p}_i^e(t_k + T|t_{k+1}) - p_i^{e*}(t_k + T|t_k) \| \le C_0 \sigma e^{aT} \tag{A3}$$

Since (17)–(25) is solved at t_k, it follows that $\| p_i^{e*}(t_k + T|t_k) \| \in \varepsilon$ holds. According to Lemma 3 and $C_0 \le \frac{e^{-aT}}{\sigma}(\delta - \varepsilon)$, it can be obtained through the triangle inequality property, that is,

$$\| \overline{p}_i^e(t_k + T|t_{k+1}) \| \le \| p_i^{e*}(t_k + T|t_k) \| + C_0 \sigma e^{aT} \le \delta \tag{A4}$$

The results show that $||\overline{p}_i^e(t_k + T|t_{k+1})|| \in \Omega_i$, for $s \in [t_k + T, t_{k+1} + T]$. According to the comparison principle, this results in

$$g_i(p_i^e(s|t_{k+1})) \le g_i(p_i^e(t_k+T|t_{k+1}))e^{-2\hat{k}(s-(t_k+T))} \tag{A5}$$

Let $s = t_{k+1} + T$, there is

$$\| \overline{p}_i^e(t_{k+1}+T|t_{k+1}) \| \le \| \overline{p}_i^e(t_k+T|t_{k+1}) \| e^{-\sigma\hat{k}} \tag{A6}$$

From Inequality (A4) and $\sigma \ge \frac{1}{\hat{k}} \ln \frac{R}{\varepsilon}$, there is $\| \overline{p}_i^e(t_{k+1}+T|t_{k+1}) \| \le \varepsilon$. Hence, (22) is satisfied at t_{k+1}.

According to

$$\| \overline{p}_i^e(s|t_{k+1}) - p_i^{e*}(s|t_k) \| \le \rho(\sigma)e^{a(s-t_{k+1})} \tag{A7}$$

there is

$$\| \overline{p}_i^e(s|t_{k+1}) \| \le \| p_i^{e*}(s|t_k) \| + C_0\sigma e^{aT} \tag{A8}$$

where $s \in [t_{k+1}, t_k+T]$. According to $C_0 \le \frac{e^{-aT}}{\sigma}(\delta-\varepsilon)$, we obtain

$$\| \overline{p}_i^e(s|t_k) \| \le \frac{T\varepsilon}{s-t_k} + (\delta-\varepsilon) \tag{A9}$$

From $\varpi\delta \le \varepsilon$, it results in $\delta \le \frac{T}{T-\sigma}\varepsilon$. In addition, there is

$$\begin{aligned} \delta-\varepsilon &\le \frac{\sigma}{T-\sigma}\varepsilon \le \frac{t_{k+1}-t_k}{s-t_k-(t_{k+1}-t_k)}\varepsilon \\ &\le \frac{t_{k+1}-t_k}{(s-t_k)(s-t_{k+1})}T\varepsilon = (\frac{1}{s-t_{k+1}} - \frac{1}{s-t_k})T\varepsilon \end{aligned} \tag{A10}$$

Substituting (A10) into Inequality (A9), we obtain $||\overline{p}_i^e(s|t_k)|| \le \frac{T\varepsilon}{s-t_{k+1}}$, $s \in [t_k + T, t_{k+1}+T]$. Considering Inequality (A5), there is

$$\| \overline{p}_i^e(s|t_{k+1}) \| \le \| \overline{p}_i^e(t_k+T|t_{k+1}) \| e^{-2\hat{k}(s-(t_k+T))} \le \delta e^{-2\hat{k}(s-(t_k+T))} \tag{A11}$$

The following functions are provided.

$$E(s) = \delta(s-t_{k+1}) - T\varepsilon e^{2\hat{k}(s-(t_k+T))} \tag{A12}$$

Replacing $E(s)$ with $s = t_k + T$, we obtain

$$E(t_k+T) = \delta(t_k+T-t_{k+1}) - T\varepsilon e^{2\hat{k}(t_k+T-(t_k+T))} < 0 \tag{A13}$$

If $\varepsilon \ge \frac{\delta}{T\hat{k}}$, there is

$$\dot{E}(s) = \delta - T\varepsilon\hat{k}e^{2\hat{k}(s-(t_k+T))} \le 0 \tag{A14}$$

where $T\hat{k} > 1$. Considering inequality (A13) with inequality (A14) yields $E(s) \le 0$, there is

$$\frac{\delta(s-t_{k+1}) - T\varepsilon e^{2\hat{k}(s-(t_k+T))}}{e^{2\hat{k}(s-(t_k+T))}(s-t_{k+1})} \le 0 \tag{A15}$$

that is, $\delta e^{-2\hat{k}(s-(t_k+T))} \le \frac{T\varepsilon}{s-t_{k+1}}$. Hence, at t_{k+1}, the state constraint (21) is satisfied.

The predicted trajectory of the *AUVi* is represented as $\overline{p}_i(s|t_{k+1}) = \hat{p}_i(s|t_{k+1})$, if the predictive control input $\overline{u}_i(s|t_{k+1}) = \hat{u}_i(s|t_{k+1})$, $s \in [t_{k+1}, t_{k+1}+T]$ is implemented. The results show that (25) is satisfied at t_{k+1}. In addition, there is

$$\pi(s|t_{k+1}) = \hat{p}_i(s|t_{k+1}) - \overline{p}_i(s|t_{k+1}) = 0 \tag{A16}$$

Therefore, at t_{k+1}, the compatibility constraint (23) is satisfied. According to the Equality (31), it yields that

$$\| \hat{p}_j(s|t_{k+1}) - \overline{p}_i(s|t_{k+1}) \| \geq R_o + \phi_{ij}(t_{k+1}),\ s \in [t_{k+1}, t_{k+1}+T] \tag{A17}$$

Thus, at t_{k+1}, (24) holds. □

The detailed proof of Theorem 2.

Proof. According to (26), the Lyapunov function is constructed as

$$V(t_k) = J_i(p_i^{e*}(t_k), u_i^{e*}(t_k)), \tag{A18}$$

$$\Delta V(t_k) = V(t_{k+1}) - V(t_k) = W_1(t_k) + W_2(t_k) + W_3(t_k) + W_4(t_k) \tag{A19}$$

where

$$W_1(t_k) = -\int_{t_k}^{t_{k+1}} (||p_i^{e*}(s|t_k)||_P^2 + ||p_{io}^{*}(s|t_k)||_R^2 + ||u_i^{e*}(s|t_k)||_S^2) ds, \tag{A20}$$

$$W_2(t_k) = \int_{t_{k+1}}^{t_k+T} (||\overline{p}_i^{e}(s|t_{k+1})||_P^2 - ||p_i^{e*}(s|t_k)||_P^2) ds \tag{A21}$$

$$\begin{aligned} W_3(t_k) \ &= \sum_{i\in N} (\sum_{j\in N_i} \int_{t_k}^{t_k+T} (||\overline{p}_{ij}(s|t_{k+1})||_Q^2 - ||p_{ij}^{*}(s|t_k)||_Q^2) ds - \int_{t_k}^{t_{k+1}} L_{ij}(p_i^{e*}(t_k), u_i^{e*}(t_k)) ds \\ &+ \int_{t_k+T}^{t_{k+1}+T} L_{ij}(p_i^{e*}(t_{k+1}), u_i^{e*}(t_{k+1})) ds + g_{ij}(p_i^{e*}(t_{k+1}+T)) - g_{ij}(p_i^{e*}(t_k+T))) \end{aligned} \tag{A22}$$

$$\begin{aligned} W_4(t_k) \ &= \int_{t_k+T}^{t_{k+1}+T} (||\overline{p}_i^{e}(s|t_{k+1})||_P^2 + ||\overline{p}_{io}(s|t_{k+1})||_R^2 + ||\overline{u}_i^{e}(s|t_{k+1})||_S^2) ds \\ &+ (||\overline{p}_i^{e}(t_{k+1}+T|t_{k+1})||_Z^2 - ||p_i^{e*}(t_k+T|t_{k+1})||_Z^2) + (||\overline{p}_{io}(t_{k+1}+T|t_{k+1})||_Z^2 - ||p_{io}^{e*}(t_k+T|t_{k+1})||_Z^2) \end{aligned} \tag{A23}$$

where $L_{ij}(p_i^e(t_k), u_i^e(t_k))$ represents the stage cost function, while $g_{ij}(p_i^e(t_k+T))$ represents the terminal cost function in the given formation. From $\| p_i^{e*}(t_{k+1}|t_k) \| > \varepsilon$, $\| u_i^{e*}(s|t_k) \|_S^2 \geq 0$, and $\| p_{io}^{*}(s|t_k) \|_R \geq R_o$, for $W_1(t_k)$, we obtain

$$W_1(t_k) \leq -\int_{t_k}^{t_{k+1}} (||p_i^{e*}(s|t_k)||_P^2 + ||p_{io}^{*}(s|t_k)||_R^2) ds \leq -\int_{t_k}^{t_{k+1}} (||p_i^{e*}(s|t_k)||_P^2 + R_o^2) ds \leq -\sigma(\lambda_{\min}(P)\varepsilon^2 + R_o^2). \tag{A24}$$

Substituting $\rho(\sigma) = C_0 \sigma e^{a\sigma}$ into the inequality $\| \overline{p}_i^e(s|t_{k+1}) - p_i^{e*}(s|t_k) \| \leq \rho(\sigma) e^{a(s-t_{k+1})}$, for $W_2(t_k)$, we obtain

$$\| \overline{p}_i^e(s|t_{k+1}) \|_P - \| p_i^{e*}(s|t_k) \|_P \leq C_0 \sigma e^{a(\sigma+s-t_{k+1})} \tag{A25}$$

From Inequality (A25), we have

$$\begin{aligned} W_2(t_k) \ &\leq \int_{t_{k+1}}^{t_k+T} 2(||\overline{p}_i^{e}(s|t_{k+1})||_P - ||p_i^{e*}(s|t_k)||_P)||p^{e*}(s|t_k)||_P + (||\overline{p}_i^{e}(s|t_{k+1})||_P - ||p_i^{e*}(s|t_k)||_P)^2 ds \\ &\leq \int_{t_{k+1}}^{t_k+T} 2\lambda_{\max}(P) C_0 \sigma e^{a(\sigma+s-t_{k+1})} ||p_i^{e*}(s|t_k)|| ds + \int_{t_{k+1}}^{t_k+T} \lambda_{\max}(P) C_0^2 \sigma^2 e^{2a(\sigma+s-t_{k+1})} ds \\ &\leq \int_{t_{k+1}}^{t_k+T} 2\lambda_{\max}(P) C_0 \sigma e^{a(\sigma+s-t_{k+1})} ||p_i^{e*}(s|t_k)|| ds + \frac{\lambda_{\max}(P) C_0^2 \sigma^2}{2a} (e^{2aT} - e^{2a\sigma}) \end{aligned} \tag{A26}$$

According to the Hölder inequality, there is

$$\begin{aligned} W_2(t_k) \ &\leq 2\lambda_{\max}(P) C_0 \sigma \left[\int_{t_{k+1}}^{t_k+T} \frac{T^2 \varepsilon^2}{(s-t_k)^2} ds \right]^{\frac{1}{2}} \left[\int_{t_{k+1}}^{t_k+T} e^{2a(\sigma+s-t_{k+1})} ds \right]^{\frac{1}{2}} + \frac{\lambda_{\max}(P) C_0^2 \sigma^2}{2a} (e^{2aT} - e^{2a\sigma}) \\ &\leq \frac{2\lambda_{\max}(P) C_0 \sigma \varepsilon}{\sqrt{2a}} \left(\frac{T^2}{\sigma} - T \right)^{\frac{1}{2}} (e^{2aT} - e^{2a\sigma})^{\frac{1}{2}} + \frac{\lambda_{\max}(P) C_0^2 \sigma^2}{2a} (e^{2aT} - e^{2a\sigma}) \end{aligned} \tag{A27}$$

For $W_3(t_k)$, the predicted position formation error is

$$\hat{p}_{ij}(s|t_k) = p_i(s|t_k) - \hat{p}_j(s|t_k) + d_{ij} \tag{A28}$$

According to the compatibility constraint (34) and triangle inequality and, there is

$$\begin{aligned}
&\sum_{i\in N}\sum_{j\in N_i}\int_{t_{k+1}}^{t_k+T}(||\overline{p}_{ij}(s|t_{k+1})||_Q^2-||p_{ij}^*(s|t_{k+1})||_Q^2)ds\\
&=\sum_{i\in N}\sum_{j\in N_i}\int_{t_{k+1}}^{t_k+T}(||p_{ij}^*(s|t_k)||_Q^2-||\hat{p}_{ij}^*(s|t_k)||_Q^2)ds\\
&\le\sum_{i\in N}\sum_{j\in N_i}\int_{t_{k+1}}^{t_k+T}(2||\hat{p}_{ij}^*(s|t_k)||_Q||\pi_j(s|t_k)||+||\pi_j(s|t_k)||_2)ds\\
&\le\sum_{i\in N}\sum_{j\in N_i}\int_{t_{k+1}}^{t_k+T}||\pi_j(s|t_k)||(2(e_{ji}(k)+\phi_{ij}(t_k))+\phi_{ji}(t_k))ds\\
&\le\sum_{i\in N}\vartheta L_{ij}(p_i^{e*}(t_k),u_i^{e*}(t_k))
\end{aligned}\tag{A29}$$

According to Assumption 3, we obtain

$$W_3(t_k)\le-\sum_{i\in N}(1-\vartheta)L_{ij}(p_i^{e*}(t_k),u_i^{e*}(t_k))\tag{A30}$$

for $W_4(t_k)$, there is

$$L_i(p_i^e(t_k),u_i^e(t_k))\le-\dot{g}_i(p_i^e(s|t_k))\tag{A31}$$

Integrating Inequality (A31) yields

$$\begin{aligned}
&\int_{t_k+T}^{t_{k+1}+T}(||\overline{p}_i^e(s|t_{k+1})||_P^2+||\overline{u}_i^e(s|t_{k+1})||_S^2)ds\\
&\le-(||\overline{p}_i^e(t_{k+1}+T|t_{k+1})||_P^2-||\overline{p}_i^e(t_k+T|t_{k+1})||_P^2)\\
&=||\overline{p}_i^e(t_k+T|t_{k+1})||_P^2-||\overline{p}_i^e(t_{k+1}+T|t_{k+1})||_P^2
\end{aligned}\tag{A32}$$

From Inequality (A3), $||\overline{p}_i^e(t_k+T|t_{k+1})||\le R$, and $||\overline{p}_i^{e*}(t_{k+1}+T|t_{k+1})||\le\varepsilon$, we obtain

$$\begin{aligned}
&\int_{t_k+T}^{t_{k+1}+T}(||\overline{p}_i^e(s|t_{k+1})||_P^2+||\overline{u}_i^e(s|t_{k+1})||_S^2)ds+||\overline{p}_i^e(t_{k+1}+T|t_{k+1})||_Z^2-||p_i^{e*}(t_{k+1}+T|t_{k+1})||_Z^2\\
&=\int_{t_k+T}^{t_{k+1}+T}(||\overline{p}_i^e(s|t_{k+1})||_P^2+||\overline{u}_i^e(s|t_{k+1})||_S^2)ds+||\overline{p}_i^e(t_{k+1}+T|t_{k+1})||_Z^2-||\overline{p}_i^e(t_k+T|t_{k+1})||_Z^2\\
&+||\overline{p}_i^e(t_k+T|t_{k+1})||_Z^2-||p_i^{e*}(t_k+T|t_k)||_Z^2\\
&\le||\overline{p}_i^e(t_k+T|t_{k+1})||_Z^2-||p_i^{e*}(t_k+T|t_{k+1})||_Z^2\\
&\le\lambda_{\max}(Z)||\overline{p}_i^e(t_k+T|t_{k+1})-p_i^{e*}(t_k+T|t_{k+1})||(||\overline{p}_i^e(t_k+T|t_{k+1})||+||p_i^{e*}(t_k+T|t_k||)\\
&\le\lambda_{\max}(Z)(R+\varepsilon)C_0\sigma e^{aT}\\
&\le2R\lambda_{\max}(Z)C_0\sigma e^{aT}
\end{aligned}\tag{A33}$$

According to Equality (7), it results in

$$\begin{aligned}
&\int_{t_k+T}^{t_{k+1}+T}||\overline{p}_{io}(s|t_{k+1})||_R^2ds+||\overline{p}_{io}(t_{k+1}+T|t_{k+1})||_Z^2\\
&\le\lambda_{\max}(R)h^2(t_{k+1}-t_k)+\lambda_{\max}(Z)h^2\le h^2(\lambda_{\max}(R)T+\lambda_{\max}(Z))
\end{aligned}\tag{A34}$$

From (A33) and (A34), we derive

$$W_4(t_k)\le2R\lambda_{\max}(Z)C_0\sigma e^{aT}+h^2(\lambda_{\max}(R)T+\lambda_{\max}(Z)).\tag{A35}$$

To sum up, it can be seen from Inequalities (A24), (A37), (A30), and (A35) that

$$\begin{aligned}
\Delta V(t_k)\le&-\sigma(\lambda_{\min}(P)\varepsilon^2+R_o^2)+\frac{\lambda_{\max}(P)C_0^2\sigma^2}{2a}(e^{2aT}-e^{2a\sigma})+\frac{2\lambda_{\max}(P)C_0\sigma\varepsilon}{\sqrt{2a}}(\frac{T^2}{\sigma}-T)^{\frac{1}{2}}(e^{2aT}-e^{2a\sigma})^{\frac{1}{2}}\\
&-\sum_{i\in N}(1-\vartheta)L_{ij}(p_i^{e*}(t_k),u_i^{e*}(t_k))+2R\lambda_{\max}(Z)C_0\sigma e^{aT}+h^2(\lambda_{\max}(R)T+\lambda_{\max}(Z))
\end{aligned}\tag{A36}$$

For $\varphi \in [0,1)$ and $L_{ij}(p_i^{e*}(t_k),\ u_i^{e*}(t_k)) \geq 0$, there is

$$-\sum_{i \in N}(1-\vartheta)L_{ij}(p_i^{e*}(t_k), u_i^{e*}(t_k)) \leq 0 \tag{A37}$$

According to Inequalities (44) and (A37), there is $\Delta V(t_k) < 0$. That is, the multi-AUV system is stable in the sense of Lyapunov using the proposed EMPC strategy under the cost function (14). □

References

1. Wang, L.; Zhu, D.; Pang, W.; Zhang, Y. A survey of underwater search for multi-target using Multi-AUV: Task allocation, path planning, and formation control. *Ocean Eng.* **2023**, *278*, 114393. [CrossRef]
2. Han, G.; Qi, X.; Peng, Y.; Lin, C.; Zhang, Y.; Lu, Q. Early warning obstacle avoidance-enabled path planning for multi-AUV-based maritime transportation systems. *IEEE Trans. Intell. Transp. Syst.* **2023**, *24*, 2656–2667. [CrossRef]
3. Deng, C.; Er, M.J. Event-triggered consensus of linear multiagent systems with time-varying communication delays. *IEEE Trans. Cybern.* **2019**, *50*, 2916–2925. [CrossRef] [PubMed]
4. Bai, C.; Yan, P.; Pan, W.; Guo, J. Learning-based multi-robot formation control with obstacle avoidance. *IEEE Trans. Intell. Transp. Syst.* **2021**, *23*, 11811–11822. [CrossRef]
5. Yang, Y.; Xiao, Y.; Li, T. A survey of autonomous underwater vehicle formation: Performance, formation control, and communication capability. *IEEE Commun. Surv. Tutor.* **2021**, *23*, 815–841. [CrossRef]
6. Dong, Y.; Huang, J. Consensus and flocking with connectivity preservation of uncertain euler-lagrange multi-agent systems. *J. Dyn. Syst. Meas. Control.* **2018**, *140*, 091011. [CrossRef]
7. Wang, D.; Zhang, N.; Wang, J.; Wang, W. Cooperative containment control of multi-agent systems based on follower observers with time delay. *IEEE Trans. Syst. Man Cybern. Syst.* **2017**, *47*, 13–23.
8. Wang, J.; Wang, C.; Wei, Y.; Zhang, C. Sliding mode based neural adaptive formation control of underactuated AUVs with leader-follower strategy. *Appl. Ocean Res.* **2019**, *94*, 101971. [CrossRef]
9. Lee, C.; Chwa, D. Decentralized behavior-based formation control of multiple robots considering obstacle avoidance. *Intel. Serv. Robot.* **2017**, *11*, 127–138. [CrossRef]
10. Yan, X.; Jiang, D.; Miao, R.; Li, Y. Formation control and obstacle avoidance algorithm of a multi-USV system based on virtual structure and artificial potential field. *J. Mar. Sci. Eng.* **2021**, *9*, 161. [CrossRef]
11. Kong, T.; Gao, H.; Yao, S.; Chen, X. Design of AUV control system based on BP neural network and PID. *Neural Comput. Adv. Appl.* **2022**, *1638*, 13–23.
12. Wang, J.; Wang, C.; Wei, Y.; Zhang, C. Filter-backstepping based neural adaptive formation control of leader-following multiple AUVs in three dimensional space. *Ocean Eng.* **2020**, *201*, 107150. [CrossRef]
13. Ferrara, A.; Incremona, G.P.; Regolin, E. Optimization-based adaptive sliding mode control with application to vehicle dynamics control. *Int. J. Robust Nonlin.* **2018**, *23*, 550–564. [CrossRef]
14. Zhang, Y.; Liu, X.; Luo, M.; Yang, C. MPC-based 3-D trajectory tracking for an autonomous underwater vehicle with constraints in complex ocean environments. *Ocean Eng.* **2019**, *189*, 106309. [CrossRef]
15. Yoo, J.; Johansson, K.H. Event-triggered model predictive control with a statistical learning. *IEEE Trans. Syst. Man, Cybern. Syst.* **2019**, *51*, 2571–2581. [CrossRef]
16. Yu, R.; Guo, H.; Sun, Z.; Chen, H. MPC-based regional path tracking controller design for autonomous ground vehicles. In Proceedings of the 2015 IEEE International Conference on Systems, Man, and Cybernetics, Hong Kong, 9–12 October 2015; pp. 2510–2515.
17. Dai, L.; Xia, Y.; Gao, Y.; Cannon, M. Distributed stochastic MPC for systems with parameter uncertainty and disturbances. *Int. J. Robust Nonlin.* **2018**, *28*, 2424–2441. [CrossRef]
18. Shen, C.; Shi, Y.; Buckham, B. Path-following control of an AUV: A multi-objective model predictive control approach. *IEEE Trans. Control. Syst. Technol.* **2019**, *27*, 1334–1342. [CrossRef]
19. Gan, W.; Zhu, D.; Hu, Z.; Shi, X.; Yang, L.; Chen, Y. Model predictive adaptive constraint tracking control for underwater vehicles. *IEEE Trans. Ind. Electron.* **2020**, *67*, 7829–7840. [CrossRef]
20. Wang, W.; Yan, J.; Wang, H.; Ge, H.; Zhu, Z.; Yang, G. Adaptive MPC trajectory tracking for AUV based on Laguerre function. *Ocean Eng.* **2022**, *261*, 111870. [CrossRef]
21. Wei, Y.; Zhu, D.; Chu, Z. Underwater dynamic target tracking of autonomous underwater vehicle based on MPC algorithm. In Proceedings of the 2018 IEEE 8th International Conference on Underwater System Technology: Theory and Applications (USYS), Wuhan, China, 1–3 December 2018; pp. 1–5.
22. Lin, X.; Gorges, D. Robust model predictive control of linear systems with predictable disturbance with application to multiobjective adaptive cruise control. *IEEE Trans. Control Syst. Technol.* **2020**, *28*, 1460–1475. [CrossRef]
23. Liu, H.; Li, X.; Fan, M.; Wu, G.; Pedrycz, W.; Suganthan, P.N. An autonomous path planning method for unmanned aerial vehicle based on a tangent intersection and target guidance strategy. *IEEE Trans. Intell. Transp. Syst.* **2020**, *23*, 3061–3073. [CrossRef]

24. Xiao, H.; Li, Z.; Chen, C.L.P. Formation control of leader-follower mobile robots' systems using model predictive control based on neural-dynamic optimization. *IEEE Trans. Ind. Electron.* **2016**, *63*, 5752–5762. [CrossRef]
25. Häusler, A.J.; Saccon, A.; Aguiar, A.P.; Hauser, J.; Pascoal, A.M. Energy-optimal motion planning for multiple robotic vehicles with collision avoidance. *IEEE Trans. Control. Syst. Technol.* **2015**, *24*, 867–883. [CrossRef]
26. Yu, J.; Dong, X.; Li, Q.; Ren, Z. Practical time-varying output formation tracking for high-order multi-agent systems with collision avoidance, obstacle dodging and connectivity maintenance. *J. Frankl. Inst.* **2019**, *356*, 5898–5926. [CrossRef]
27. Wang, P.; Ding, B. A synthesis approach of distributed model predictive control for multi-agent system with collision avoidance. *Int. J. Control.* **2014**, *87*, 52–63. [CrossRef]
28. Tallamraju, R.; Rajappa, S.; Black, M.J.; Karlapalem, K.; Ahmad, A. Decentralized MPC based obstacle avoidance for multi-robot target tracking scenarios. In Proceedings of the 2018 IEEE International Symposium on Safety, Security, and Rescue Robotics (SSRR), Philadelphia, PA, USA, 6–8 August 2018; pp. 1–8.
29. Yang, Y.; Ding, B. Tracking and formation of multi-agent systems with collision and obstacle avoidance based on distributed RHC. *Circuits Syst. Signal Process.* **2018**, *38*, 2951–2970. [CrossRef]
30. Shen, C.; Shi, Y.; Buckham, B. Model predictive control for an AUV with dynamic path planning. In Proceedings of the 2015 54th Annual Conference of the Society of Instrument and Control Engineers of Japan (SICE), Hangzhou, China, 28–30 July 2015; pp. 475–480.
31. Hu, Q.; Xie, J.; Wang, C. Dynamic path planning and trajectory tracking using MPC for satellite with collision avoidance. *ISA Trans.* **2019**, *84*, 128–141. [CrossRef]
32. Ji, J.; Khajepour, A.; Melek, W.W.; Huang, Y. Path planning and tracking for vehicle collision avoidance based on model predictive control with multiconstraints. *IEEE Trans. Veh. Technol.* **2017**, *66*, 952–964. [CrossRef]
33. Zuo, Z.; Yang, X.; Li, Z.; Wang, Y.; Han, Q.; Wang, L.; Luo, X. MPC-based cooperative control strategy of path planning and trajectory tracking for intelligent vehicles. *IEEE Trans. Intell. Veh.* **2021**, *6*, 513–522. [CrossRef]
34. Liu, S.; Luo, W.; Wu, L. Co-design of distributed model-based control and event-triggering scheme for load frequency regulation in smart grids. *IEEE Trans. Syst. Man, Cybern. Syst.* **2020**, *50*, 3311–3319. [CrossRef]
35. Wang, L.; Zhu, D.; Pang, W.; Luo, C. A novel obstacle avoidance consensus control for multi-AUV formation system. *IEEE/CAA J. Autom. Sin.* **2023**, *10*, 1304–1318. [CrossRef]
36. Yang, H.; Li, Q.; Zuo, Z.; Zhao, H. Event-triggered model predictive control for multi-vehicle systems with collision avoidance and obstacle avoidance. *Int. J. Robust Nonlinear Control.* **2021**, *31*, 5476–5494. [CrossRef]
37. Dai, L.; Cao, Q.; Xia, Y.; Gao, Y. Distributed MPC for formation of multi-agent systems with collision avoidance and obstacle avoidance. *J. Frankl. Inst.* **2017**, *354*, 2068–2085. [CrossRef]
38. Gan, W.; Zhu, D.; Ji, D. QPSO-model predictive control based approach to dynamic trajectory tracking control for unmanned underwater vehicles. *Ocean Eng.* **2018**, *158*, 208–220. [CrossRef]
39. Wang, P.; Ding, B. Distributed RHC for tracking and formation of nonholonomic multi-vehicle systems. *EEE Trans. Autom. Control.* **2014**, *59*, 1439–1453. [CrossRef]
40. Sun, Z.; Dai, L.; Liu, K.; Xia, Y.; Johansson, K.H. Robust MPC for tracking constrained unicycle robots with additive disturbances. *Automatica* **2018**, *90*, 172–184. [CrossRef]
41. Sun, Z.; Xia, Y. Receding horizon tracking control of unicycle-type robots based on virtual structure. *Int. J. Robust Nonlinear Control.* **2016**, *26*, 3900–3918. [CrossRef]
42. Miao, J.; Wang, S.; Zhao, Z.; Li, Y.; Tomovic, M. Spatial curvilinear path following control of underactuated AUV with multiple uncertainties. *ISA Trans.* **2017**, *67*, 107–130. [CrossRef]